Lab on a Chip

PAPER

View Article Online
View Journal

Cite this: DOI: 10.1039/c4lc01179a

Biophysical properties of human breast cancer cells measured using silicon MEMS resonators and atomic force microscopy†

Elise A. Corbin,[ab] Fang Kong,[c] Chwee Teck Lim,[cdef] William P. King[ab] and Rashid Bashir*[bg]

Received 6th October 2014,
Accepted 28th November 2014

DOI: 10.1039/c4lc01179a

www.rsc.org/loc

Biophysical studies on individual cells can help to establish the relationship between mechanics and biological function. In the case of cancer, mechanical properties of cells have been linked to metastatic activity and disease progression and can be crucial for understanding cellular physiology and metabolism. In this study, we report measurements of the stiffness of breast cancer cells using a novel silicon MEMS resonant sensor and validated the results with atomic force microscopy (AFM). We measured the mass and stiffness of individual benign (MCF-10A), non-invasive malignant (MCF-7), and highly-invasive malignant (MDA-MB-231) breast cancer cells using the silicon resonant MEMS sensors. The sensor extracts the average stiffness value of the whole cell and allows comparison of stiffness of different cell types. We found differences between the cell lines in both elasticity and viscosity, and confirmed our observations through independent measurements with atomic force microscopy (AFM). Coupled with measurements over time, this approach could lead to a multimodal investigation of both growth and physical properties of single cells. The mechanical property sensitivity and resolution of these pedestal sensors were investigated to understand the significance of the frequency shift during operation. The lowest achievable spring constant and damping constant resolutions have a range of 0.06 to 17.10 mN m^{-1} and 1.63 to 1.96 nN s m^{-1}, respectively, measured across the range of physiological cell mechanical properties.

Introduction

A cell is a complex dynamic system with highly integrated structure and function. Cellular mechanics relates to both aspects; the mechanical properties of cells allow the cell to withstand the physiological environment in which they live, and also dictate the response to mechano-signaling pathways. Deviations in mechanical properties will influence biological behavior, such as cellular growth, differentiation, spreading, migration, and apoptosis. Given the overarching view of the health of the cell provided by its mechanics, quantification of the mechanical properties of individual cells has been an active area of research. Studies on the viscoelasticity of individual cells have largely focused on cancer cells given the potential to elucidate mechanisms of disease onset and progression.

It is well known that cells differ in their viscoelastic properties depending on their health.[1] This is especially true in cancer cells, which are soft compared to their normal counterparts,[2] but also for other diseased cells including malaria-infected red blood cells which are stiffer than uninfected red blood cells.[3] The relative softness of cancer cells has been linked to heightened invasiveness due to their increased deformability,[4] which, when coupled with reduced adhesion,[5] enables cancer cells to escape to other tissues and metastasize. Viscoelasticity also plays a role in how cells interact with their environment, and the differences in their physical properties may influence mechanical signaling pathways that could result in some of the hallmark aspects of cancer behavior.[6]

A variety of methods exist for probing the mechanical properties of individual living cells, including atomic force microscopy,[7] magnetic twisting cytometry,[8] micropipette aspiration,[9] and optical trapping.[10] However, the development of

[a] Department of Mechanical Science and Engineering, University of Illinois Urbana-Champaign, Urbana, IL 61801, USA
[b] Micro and Nanotechnology Laboratory, University of Illinois Urbana-Champaign, Urbana, IL 61801, USA. E-mail: rbashir@illinois.edu
[c] Singapore-MIT Alliance for Research and Technology, National University of Singapore, Singapore
[d] Department of Biomedical Engineering, National University of Singapore, Singapore
[e] Mechanobiology Institute, National University of Singapore, Singapore
[f] Department of Mechanical Engineering, National University of Singapore, Singapore
[g] Department of Bioengineering, University of Illinois Urbana-Champaign, Urbana, IL 61801, USA

† Electronic supplementary information (ESI) available. See DOI: 10.1039/c4lc01179a

techniques and devices for cellular stiffness measurement remains an active area of investigation. In particular, there is a need for a fast, high throughput method to capture the mechanical properties of a cell under varying conditions. How a cell interacts mechanically with its microenvironment is dependent on its stiffness, and this affects mechano-signaling cues that influence behavior, including cellular growth.[1,11] Recently, the development of technologies for measuring the mass of individual cells has enabled studies of cellular growth rate.[12] These studies use the resonant frequency of MEMS sensors to extract the mass of cells added to the system.[13] Previously, we have demonstrated that the viscoelasticity of objects adhered on resonant sensors also produces a predictable shift in resonant frequency that can be used to extract mechanical properties.[14] By developing methods to probe cellular viscoelasticity through resonant frequency shift, there is potential for multiple biophysical measurements on a single chip.

In this study, we report measurements of the mechanical properties of breast cancer cells using silicon MEMS resonant sensors through the shift in resonant frequency associated with viscoelasticity of adhered objects. Here, we investigate the stiffness of individual benign (MCF-10A), non-invasive malignant (MCF-7), and highly-invasive malignant (MDA-MB-231) human breast cancer cells. The relationships between different cell lines are verified through independent measurements of viscoelasticity from atomic force microscopy (AFM). The arrayed format of these devices can provide high throughput measurements of the whole cell viscoelastic properties, with high achievable resolution in determining mechanical properties. Using resonant sensors to measure viscoelasticity may ultimately lead to simultaneous studies of cellular growth and mechanical properties.

Results and discussion

MEMS resonant sensors use resonant frequency shift to measure the mass of adhered objects; however, in principle, these devices are capable of measuring any physical property that affects resonant frequency. For instance, when soft cells are adhered to the sensors, they vibrate out-of-phase with the platform and the resonant frequency shift is affected by both their mass and viscoelasticity. We model this behavior using a two degree-of-freedom (2DOF) system with the cell as a Kelvin–Voigt viscoelastic material attached to a spring-mass-damper system representing the resonant sensor. A Kelvin–Voigt material consists of a mass attached to a spring and damper in parallel, and is accepted as an appropriate model for cellular behavior.[15]

Fig. 1 provides an overview of the measurement theory behind the resonant shift effect from material viscoelasticity.[13a,14] Details of the resonant sensors and experimental setup used in this study are described elsewhere.[13a,16] Briefly, the resonant sensor employed is a 60 × 60 μm^2 pedestal suspended by four beam-springs (Fig. 1A and B) that provide uniform sensitivity to frequency shift, regardless of adherent cell position, and we array them in a 9 × 9 format of 81 sensors.[13a,16] Our experimental setup includes a magnetic field to induce a first order motion, a camera to provide a control mechanism, and a feedback system to measure a sensor resonant frequency. This system naturally drifts over time and empty sensors are used to correct for the resonant frequency drift. Fig. 1C presents the 2DOF model from which the additional shift in resonant frequency beyond that associated with object mass is predicted. Fig. 1D shows the general shape of the behavior predicted by the model, where at low elasticity and low viscosity there will be a significant additional frequency shift. In the case of stiff materials with high elasticity or viscosity, this effect is minimized and the entire measured frequency shift can be attributed to mass.

Extracting information about viscoelasticity from resonant frequency shift requires a method to remove the contributions from object mass, typically by obtaining a reference "true mass" value.[14] In the case of cells, this reference value can be obtained by measuring the resonant frequency after making the object very stiff, such as through fixation.[17] The experimental protocol for investigating cellular viscoelasticity consisted of two separate measurements of resonant

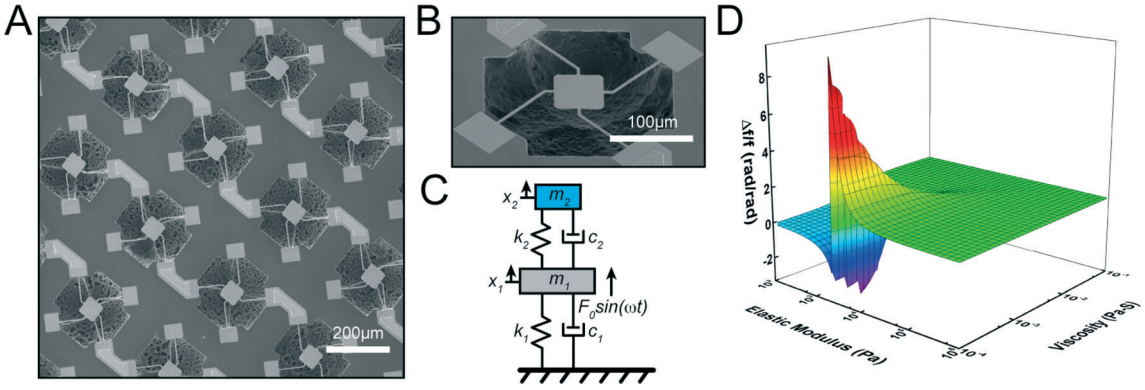

Fig. 1 Overview of the measurement theory. (A) Scanning electron microscope image of the sensor array. (B) Scanning electron microscope image of a single sensor. (C) Free-body-diagram of the two-degree-of-freedom system model. (D) An example of a result from the 2DOF model, a three-dimensional plot summarizing how cell stiffness (elastic modulus) and viscosity influence frequency response measurement.

frequency with adhered cells both before and after fixation. After measuring the frequency shift after live cells are seeded on the sensor, we fixed the cells with 4% paraformaldehyde for 30 min. Before taking the next measurement, we completely flushed the fixative solution and replaced it with growth media to match the first measurement. The second frequency measurement was then acquired and compared with the pre-fixation measurement. Fig. 2A shows the relationship between live and fixed resonant frequency shift measurements for each measured cell. There is a clear discrepancy between the two values, with the fixation procedure resulting in lower resonant frequencies from greater shifts. According to the model in Fig. 1D, the out-of-phase vibration of very soft materials will actually result in a negative resonant frequency shift, thus causing measurements after fixation to be much greater.

The amplitude of the resonant frequency difference pre- and post-fixation can also be used to determine how soft cells are. Fig. 2A shows fitted trend lines for each measured cell line – MCF-10A, MFC-7, and MDA-MB-231 – with the slope representing the ratio between fixed and live frequency shift. MDA-MB-231 has the largest discrepancy between the two measurements with a slope of 1.58, followed by MCF-7 with a slope of 1.27 and MCF-10A with a slope of 1.16. Fig. 2B compares these slopes and their 95% confidence intervals from each linear regression, along with the ranges of individual cell ratios. Referring to the model in Fig. 1D, it is clear that each of the cells has different mechanical properties, with MDA-MB-231 being the softest cell line and MCF-10A the stiffest.

From the pre- and post-fixation measurements and the 2DOF model, we estimated the viscoelastic properties of each cell line using a previously introduced procedure[14] that will only be briefly described here. The property estimation uses the forward model of expected frequency shift for a set of properties to formulate an error term describing the difference between expected and measured shifts for all cells from a given line. This error term is then minimized through iterative updating of both material elasticity and viscosity to determine the cell line group average properties. Population variability in elasticity and viscosity was estimated from variability in pre- and post-fixation ratios. From these measurements, we found that MCF-10A cells are the stiffest, with an elastic modulus of 398.1 ± 104.1 Pa, followed by MCF-7 at 275.2 ± 157.4 Pa and MDA-MB-231 at 257.5 ± 98.4 Pa. These findings agree with previous reports of breast cancer cells being softer with malignancy,[2b] and that invasiveness is reflected through reduced stiffness.[4a] MCF-10A cells also have the highest viscosity of 10.2 ± 2.7 mPa s, though MDA-MB-231 is more viscous than MCF-7 (8.1 ± 3.1 *vs.* 7.4 ± 4.2 mPa s). The observation of lower viscosity in malignant breast cancer cells has been previously reported,[2b,18] though a recent study has suggested that reduced viscosity is not a marker for invasiveness,[19] which is reflected in our measured properties. Given the nature of the measurement technique, we are unable to determine the statistical significance of our observed mechanical properties. Instead, we sought to verify our measurements through an additional biomechanical analysis technique.

We used AFM as an independent method to verify the stiffness relationships observed using the resonant sensors. AFM is a widely used technique for nanoindentation measurements of cellular mechanical properties, including elasticity and viscosity. Measurements on each cell consisted of 64 indentations arranged in a grid, each resulting in calculated property values. To determine the average properties across all cells in a given line, we collectively analyzed the results from each point-wise indentation. Fig. 3 presents histograms of elastic modulus measurements for each cell line, both pre- and post-fixation, along with the fitted lognormal distributions.[20] Fig. 4 similarly shows histograms of the measured creep time constant, which is used to calculate material viscosity.

Fig. 5 summarizes the results of AFM measurements for each investigated cell line for comparison with the previous findings. The mean and standard deviation for each property

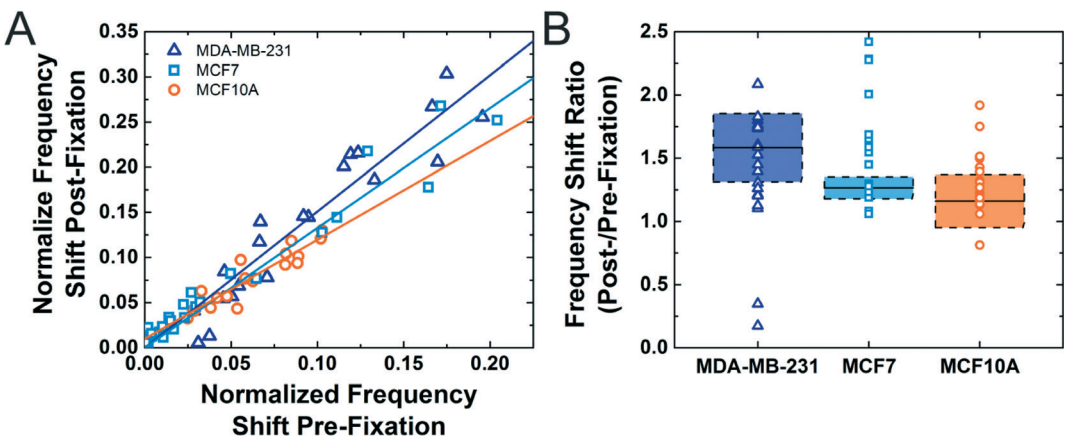

Fig. 2 The normalized frequency shift comparison after to before fixation ratio. (A) The frequency resonant shift of MDA-MB-231, MCF-7, and MCF-10A cells after fixation are 1.58, 1.26, and 1.16, times greater than before fixation, respectively. (B) Statistics of the frequency shift values on a box plot.

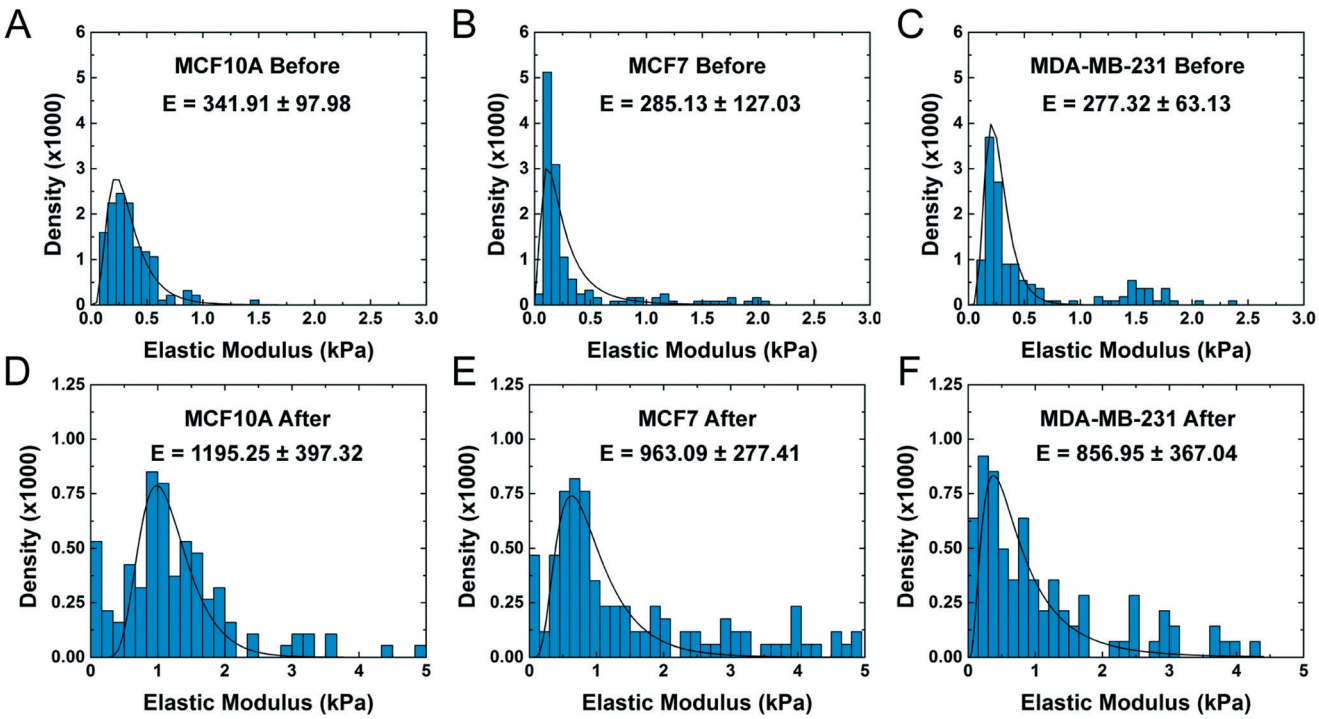

Fig. 3 (A–F) Results from AFM mechanical measurements both before and after fixation performed on MDA-MB-231, MCF-7, and MCF-10A cells. Elastic modulus values were extracted from the force-displacement measurements. Histograms of the elastic modulus with lognormal fits for MDA-MB-231, MCF-7, and MCF-10A both before and after fixation.

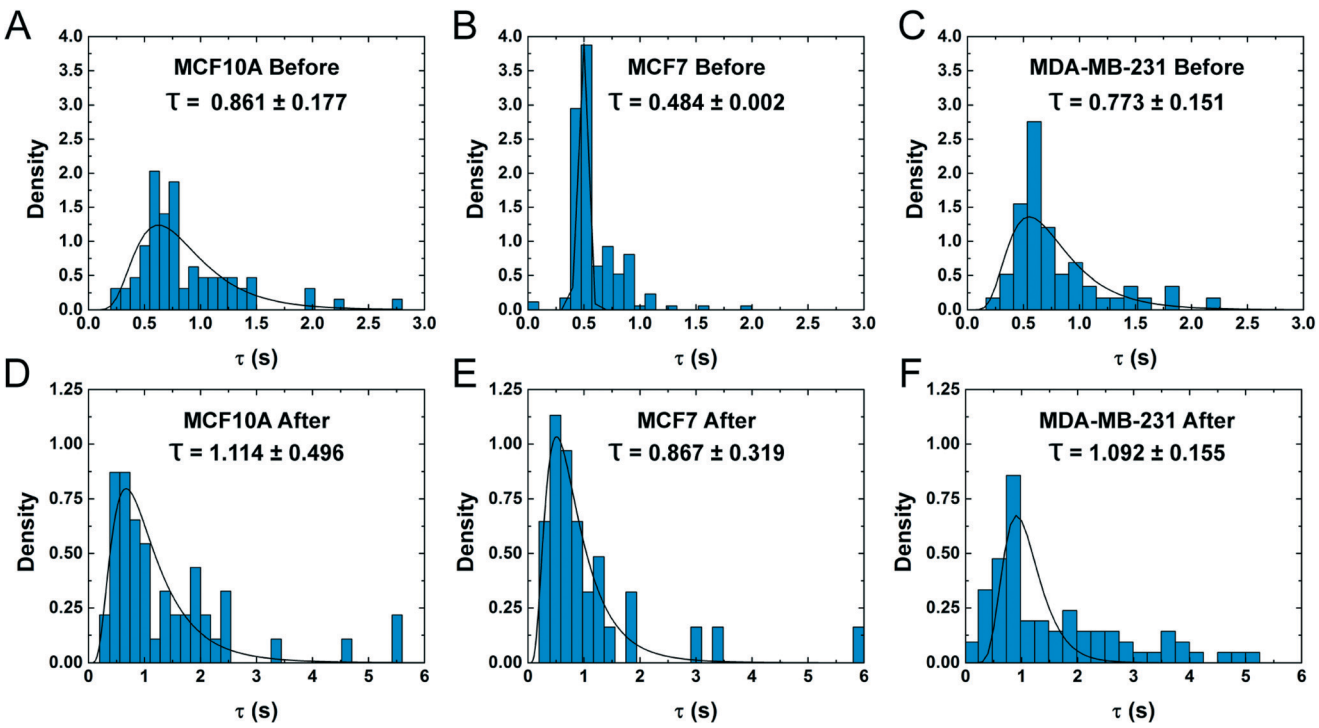

Fig. 4 (A–F) Results from AFM mechanical measurements both before and after fixation performed on MDA-MB-231, MCF-7, and MCF-10A cells. Viscosity scaling time values were extracted from force-displacement measurements with a dwell period on the surface when performing this creep test. Histograms of the elastic modulus with lognormal fits for MDA-MB-231, MCF-7, and MCF-10A both before and after fixation.

are determined through the lognormal distribution of indentation measurements. The elastic modulus of the cells ranges from 270 Pa to 340 Pa before fixation to 800 Pa to 1200 Pa after fixation. In both states, we found that MDA-MB-231 was

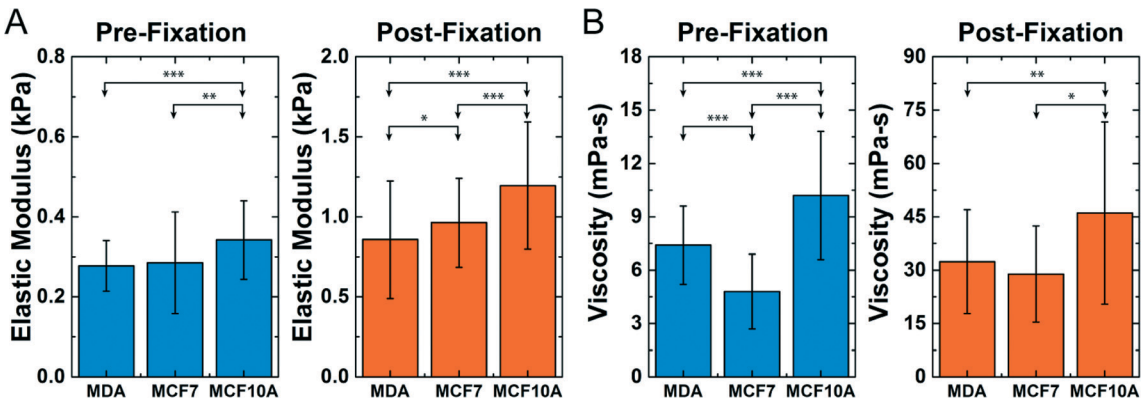

Fig. 5 Results from AFM mechanical measurements both before and after fixation performed on MDA-MB-231, MCF-7, and MCF-10A cells. Comparison of (A) elastic modulus values, and (B) viscosity values had been compensated for dependence on frequency estimated at 60 kHz.

the softest of the cell lines followed by MCF-7 and then MCF-10A. Viscosity values exhibited a trend similar to the elastic moduli, with the viscosities of the cancer cells being lower than the benign cells. However, as in the viscosities estimated from the resonant sensor, the highly-invasive malignant cell had a larger viscosity value than the non-invasive malignant cell. Viscosity pre-fixation ranged between 5 mPa s to 9 mPa s, while viscosity post-fixation ranged between 22 mPa s to 46 mPa s. The post-fixation elastic modulus and viscosity values confirm the assumption that there is minimal contribution to resonant frequency shift from viscoelasticity of the fixed cells.

Despite our findings in cells known to exhibit different invasiveness, it is not appropriate to draw general conclusions about invasiveness and viscoelasticity from our measurements. In order to investigate such a relationship, cell lines cultured to promote differing levels of invasiveness, such as the B16-F1 through-F10 murine melanoma cancer lines,[21] must be compared. One example is a recent study on the mechanics of malignant colorectal cancer cells with AFM, which found that invasive cells exhibited greater stiffness than their non-invasive, tumorigenic counterparts.[22] Comparing this finding with our results suggests that invasiveness may not be the primary cause of viscoelastic differences, but rather other aspects of the cell structure that could be implicated in invasiveness and cancerous behavior.

Table 1 collects the viscoelastic properties of each cell line determined by AFM and from the resonant sensor. The two techniques show remarkable agreement, with both capturing the same trends in stiffness and viscosity with malignancy and metastatic potential. In previous works, we used the resonant sensors to estimate absolute values for object stiffness;[13a,14] however, accurate estimation requires *a priori* knowledge of object shape as an input to the 2DOF model. When cells have a low profile, *i.e.* the cells are relatively flat on the surface, their viscoelasticity can have a reduced effect on resonant frequency, even when very soft.[13b] This can explain why the MDA-MB-231 cells cause a greater frequency shift due to viscoelasticity than MCF-7 cells, though the mechanical properties of the two cell lines are more similar, suggesting that MDA-MB-231 cells have a different shape that influences resonant frequency shift.

Table 1 Compares the values obtained from atomic force microscopy and the MEMS resonant sensor

	Atomic force microscopy		MEMS resonant sensor	
Cell type	Elastic	Viscous	Elastic	Viscous
MCF-10A	341.9 ± 98	10.2 ± 3.6	398.1 ± 104.1	10.2 ± 2.7
MCF-7	285.1 ± 127	4.8 ± 2.1	275.2 ± 157.4	7.4 ± 4.2
MDA-MB-231	277.3 ± 63.1	7.4 ± 2.2	257.5 ± 98.4	8.1 ± 3.1

For estimating cell shape in order to perform the material property estimation, we used confocal microscopy to image cells from each investigated line. Fig. 6 presents lateral and axial confocal images of individual cells, demonstrating the different ratios of base area to profile height between cell types. We measured the area to height ratio from confocal microscopy images for approximately fifteen cells from each line, and found that MCF-7 cells have a smaller area to height ratio than MDA-MB-231 cells (Fig. 6D). This ultimately results in MCF-7 having a smaller spring constant, which is a property of the object dependent on its shape, despite having very similar material mechanical properties.

The resonant frequency shift due to material properties is more appropriately described as due to the effective spring and damping constants of the object, k and c, as these are the components of the 2DOF model (Fig. 1). We can define the sensitivity of the resonant sensor in detecting spring constant by how it changes the resonant frequency, $S_k = \Delta f/\Delta k$. Similarly, the sensitivity to damping constant is $S_c = \Delta f/\Delta c$. However, referring to Fig. 1D, it is clear that these sensitivities are actually functions of both k and c. Fig. 7A and B show the sensitivities, $S_k(k, c)$ and $S_c(k, c)$, over a range of parameter values. We can further calculate the minimum detectable parameter change, or the resolution of the spring and damping constant estimates, through the minimum detectable frequency shift. The frequency shift resolution indicates the smallest step change that could be measured in a given integration time and can be determined by the noise,

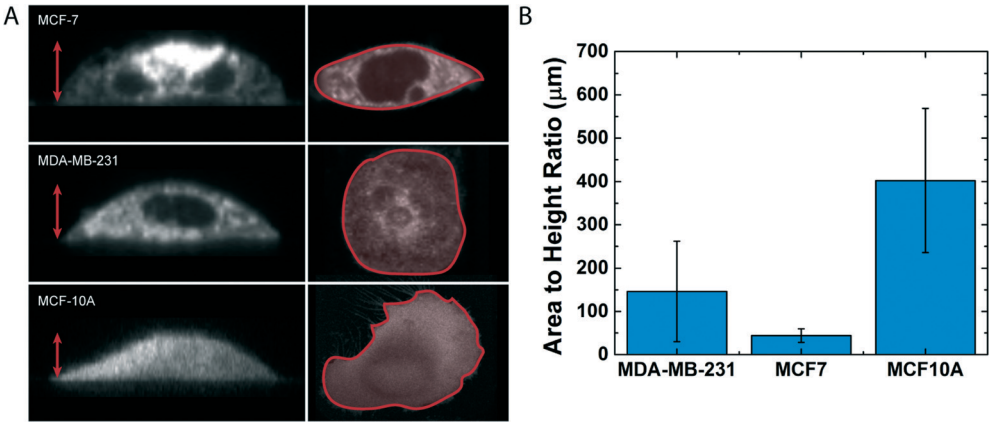

Fig. 6 (A) Lateral and axial confocal images of MCF-7, MDA-MB-231, and MCF-10A cells showing the height and contact area diameter of each cell type. (B) Radius to height ratios for MCF-7 and MDA-MB-231 cells found through the forward 2DOF problem.

or average uncertainty *Uavg*. For the sensors used in this work, the uncertainty in frequency shift is 1.23 Hz[13a] that can be combined with the sensitivity, *S*, to define the resolution in *k* and *c* as *Uavg*/*S*. Fig. 7C and D show the resulting best *k* and *c* resolutions. We found that for the range of parameters determined through AFM and confocal microscopy, the spring constant resolution has a range of 0.06 to 17.10 mN m^{-1} and the damping constant resolution has a range of 1.63 to 1.96 nN s m^{-1}. The spring constant resolutions that we achieve are comparable to techniques such as AFM that ranges from 0.4291 mN m^{-1} to 1.9365 mN m^{-1} for the values obtained in this paper.

For studying the mechanical properties of individual living cells, the resonant sensors employed in this work exhibit sensitivity to differences in mechanical properties between cell lines. However, this sensitivity is confined to materials that have viscoelastic properties within a certain range (Fig. 7A and B), which limits the ability to study a greater set of materials. The extent of this region depends on the properties of the sensor, including its mass, spring constant, and surrounding medium. By modifying these characteristics in the design, the sensitivity of the device can be tailored for a specific application.

Many methods exist for measuring the viscoelasticity of cells. Microindentation with AFM is rapidly becoming the most popular tool for studying living cells because of the excellent sensitivity of microcantilevers. However, there are challenges to using AFM that limit its utility in many applications. This is reflected in the reported cellular elastic modulus values varying by orders of magnitude. AFM relies on certain assumptions regarding the cell being soft, thin, irregularly shaped, and submerged in fluid, which make interpreting the contact point and force-distance curves difficult due to noise and lack of clear discontinuity. Careful experiments that consider these factors in measuring viscoelasticity are a time-consuming effort, and the overall number of cells to be reliably analyzed can be limited. Because of the poor throughput of AFM measurements, the ability to synchronize readings across a population or with other biological and biochemical phenomena is ultimately compromised.

MEMS resonant sensors are an attractive alternative to the traditional cell mechanical characterization methods because of their scalability, fast response time, high-throughput, and the ability to operate in either liquid or gaseous environments. Fabrication is relatively simple since no tip is needed, and one chip can contain many devices arranged in large arrays for simultaneous measurements. Additionally, the pedestal resonant sensors used in this work provide a uniform frequency response independent of cell position, and their structure reduces the necessary stress deflection that is a challenge in the fabrication and use of cantilevered devices. The need for a separate volume measurement does not limit throughput as it is an independent step, and such a measurement is not necessary for every experiment after the initial estimation of population shape. Although our measurements currently take advantage of a single shape estimate for the entire cell population, individual shape estimates can be included in future versions of the system through the incorporation of the appropriate optical system, and thus improve the accuracy of our property measures. Ultimately, these devices provide a fast and easy way to measure the whole cell mechanical properties, which introduces the potential for measuring the change in viscoelasticity over time.

Conclusions

The mechanisms relating the mechanical properties of cells to state of disease and how they grow and progress through the cell cycle remain an open area of investigation. These mechanisms are especially critical in studies of cancer where the cell cycle is disrupted and altered biophysical properties influence mechanical signaling through micro-environmental interactions. In this work, we used a new MEMS resonant sensor to investigate the viscoelastic properties of human breast cancer cell lines. We clearly demonstrate through the 2DOF model extraction that the MEMS resonant sensor is

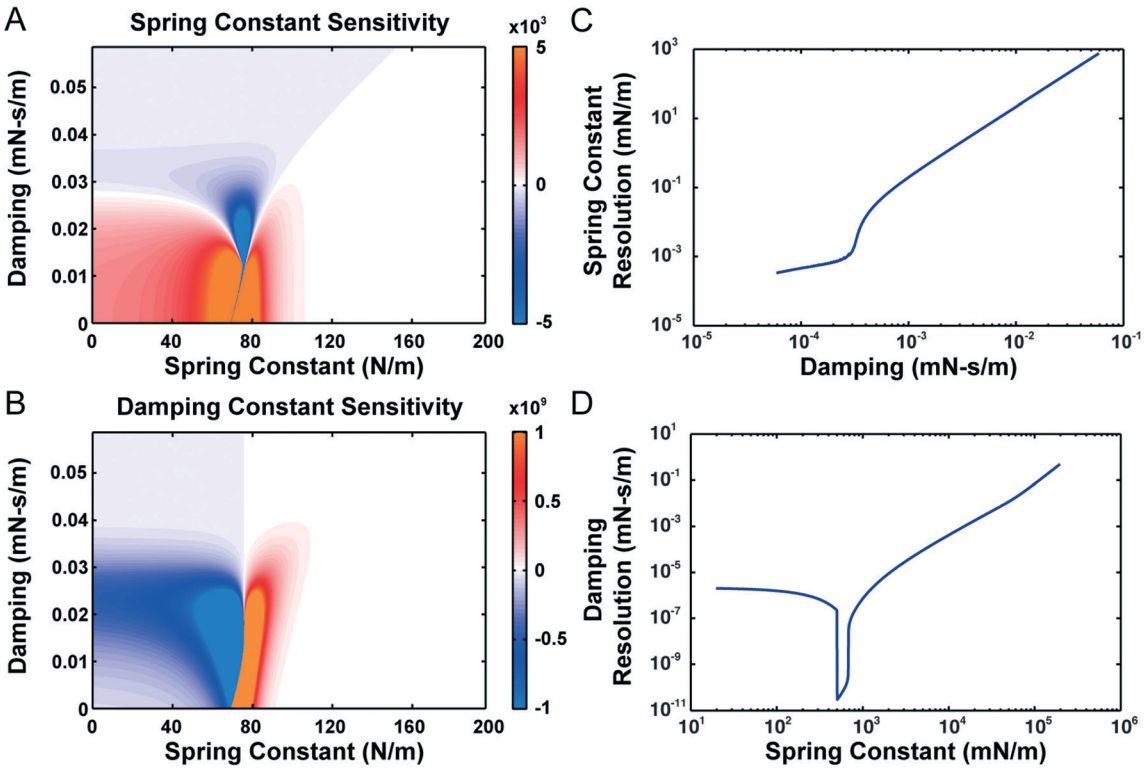

Fig. 7 (A) Spring constant sensitivity, $S_k(k, c)$, over a range of parameter values, which is found by taking the derivative of the frequency change with respect to the spring constant. (B) Damping constant sensitivity, $S_c(k, c)$, over a range of parameter values, which is found by taking the derivative of the frequency change with respect to the damping constant. (C) Spring constant resolution is the minimum detectable change in frequency that corresponds to a spring constant, which is found to be 0.06 to 17.10 mN m^{-1}, for the found range of cell physiological properties through AFM. (D) Damping resolution is the minimum detectable change in frequency that corresponds to a damping constant, which is found to be 1.63 to 1.96 nN s m^{-1}, for the found range of cell physiological properties through AFM.

capable of detecting differences in the mechanical properties between cell lines that vary in malignancy and invasiveness, and validated these observations through independent measurements with AFM. The resolution of our sensor, system, and model combined is sufficiently low to measure minute changes in the mechanical properties of a cell. This technique will enable sensitive measurements for biophysical studies of environmental changes on a cell, which could prove invaluable in studying the role of signaling in cancer.

Experimental section

Cell culture and fixation protocol

Normal human breast epithelial cells (MCF-10A) were cultured in Dulbecco's Modified Eagle Medium/Ham's F-12 (Gibco) with 5% horse serum, 20 ng mL^{-1} EGF, 0.5 mg mL^{-1} hydrocortisone, 100 ng mL^{-1} cholera toxin, 10 μg mL^{-1} insulin, and 1% penicillin streptomycin. Human breast adenocarcinoma cells (MCF-7) were cultured in Dubecco's Modified Eagle Medium (Gibco) with 10% fetal bovine serum and 1% penicillin streptomycin. Highly-invasive malignant human breast adenocarcinoma cells (MDA-MB-231) were cultured in Leibovitz's L-15 Medium (Sigma-Aldrich) with 10% fetal bovine serum and 1% penicillin streptomycin.

We selectively functionalized the sensor area of the device with type I collagen and backfilled the rest of the area with pluronic to repel cell adhesion, details of the select functionalization and passivation used in this study are described elsewhere.[23] Cells were initially seeded onto the sensors at a total of 9000 cells per chip and allowed to adhere. After cells adhered to the sensor area, the sensors were rinsed with fresh growth media to remove non-adhered cells and the culture chamber was sealed with a sterilized glass cover slip for the measurement. Resonant frequency measurements were taken of the sensors with live cells captured (see Fig. S1†). After the live measurements, the cells were fixed with 4% paraformaldehyde for 30 min. The fixative solution was completely flushed and replaced with growth media, and the resonant frequency of each sensor with a fixed cell was measured.

Mechanical property characterization

A NanoWizard® 3 (JPK Instruments AG; Berlin, Germany) atomic force microscope (AFM) was used to characterize the mechanical properties of MCF-10A, MCF-7, and MDA-MB-231 cells. We used a silicon nitride cantilever with a spring constant of 0.006 N m^{-1} and a 4.5 μm silica spherical indenter to extract force-indentation curves. The cells were seeded on collagen type I treated glass coverslip that was attached to

the base of a Petri dish with Norland optical adhesive. The adhesive was cured using a BioForce Nanosciences UV/Ozone cleaner for 10 min, prior to collagen deposition and cell seeding.

Force-distance curves were taken at 64 points (8 × 8) over the entire cell structure. The elastic modulus of the each point on the cell was extracted from the region of elastic deformation using the Hertz model (Fig. S2A†). In this case, the material properties of the spherical indenter particle, the elastic moduli and Poisson ratio, are 68 GPa and 0.19, respectively. The elastic modulus of each cell is reported as the median of all 64 measured points. Three cells from each cell line were measured both live and after fixation with 4% paraformaldehyde, as described above for the mass measurements.

The viscosity of each cell, both before and after fixation, was calculated from creep indentation measurements with AFM using the same cantilever and indenter tip (Fig. S2B†). A step load was applied to the cantilever probe and the resulting applied force was held constant for ten seconds through a feedback loop on the cantilever deflection. While the force was held constant, the cantilever Z-sensor signal was monitored to collect a creep curve, and extract the material viscosity using the Kelvin–Voigt model. Once the low frequency viscosity is obtained from the creep measurements, we need to adjust the effective viscosity to account for both frequency dependence and the high frequency of oscillation in the experiment.

The Kelvin–Voigt model uses the material viscosity to describe the imaginary part of the complex elastic modulus, $E = E' + iE''$, along with the oscillation frequency, ω:

$$E = E' + i\omega\eta. \quad (1)$$

However, the imaginary elastic modulus is also frequency-dependent and generally obeys a power-law relationship:

$$E''(\omega) = E_0''\omega^{\alpha} \quad (2)$$

Combining the two equations, and assuming an α of 0.2,[24] we derive an expression for the effective viscosity at a frequency of 60 kHz, relative to the nominal viscosity, η_0:

$$\eta_{60\ \mathrm{kHz}} = \frac{\eta_0}{2\pi(60\ \mathrm{kHz})^{1-\alpha}}. \quad (3)$$

Confocal measurements

Confocal microscopy was used to determine volume, height, and shape ratio of a population of patterned single cells labeled with lipophilic fluorescent dye DiOC6(3) (3 μL mL^{-1}) and immersed in PBS. Confocal image stacks (Z-stacks) were acquired with a Zeiss 710 laser scanning confocal microscope using an Argon laser (488 nm) and a 40× water immersion objective (Carl Zeiss Microscopy GmbH; Jena, Germany). To ensure that the Z-stacks represented the cell dimensions accurately in three-dimensions, *XYZ* voxel size (X = 0.21 μm, Y = 0.21 μm, Z = 0.46 μm) was set based on Nyquist criteria (two pixels per actual unit resolution in *XYZ*). Amira 5.4.1 (Visualization Sciences Group; Merignac, France) was used to measure cell height and base area from confocal images.

Acknowledgements

E.A.C. was funded at UIUC from NSF Grant 0965918 IGERT: Cellular and Molecular Mechanics and BioNanotechnology.

References

1 G. Bao and S. Suresh, *Nat. Mater.*, 2003, **2**, 715–725.
2 (*a*) S. E. Cross, Y.-S. Jin, J. Rao and J. K. Gimzewski, *Nat. Nanotechnol.*, 2007, **2**, 780–783; (*b*) Q. S. Li, G. Y. H. Lee, C. N. Ong and C. T. Lim, *Biochem Biophys. Res. Commun.*, 2008, **374**, 609–613.
3 (*a*) D. Fedosov, B. Caswell, S. Suresh and G. Karniadakis, *Proc. Natl. Acad. Sci. U. S. A.*, 2011, **108**, 35–39; (*b*) S. Suresh, J. Spatz, J. Mills, A. Micoulet, M. Dao, C. Lim, M. Beil and T. Seufferlein, *Acta Biomater.*, 2005, **1**, 15–30.
4 (*a*) W. Xu, R. Mezencev, B. Kim, L. Wang, J. McDonald and T. Sulchek, *PLoS One*, 2012, **7**, e46609; (*b*) S. Byun, S. Son, D. Amodei, N. Cermak, J. Shaw, J. H. Kang, V. C. Hecht, M. M. Winslow, T. Jacks and P. Mallick, *Proc. Natl. Acad. Sci. U. S. A.*, 2013, **110**, 7580–7585.
5 (*a*) U. Cavallaro and G. Christofori, *Nat. Rev. Cancer*, 2004, **4**, 118–132; (*b*) J. S. Desgrosellier and D. A. Cheresh, *Nat. Rev. Cancer*, 2010, **10**, 9–22.
6 (*a*) D. T. Butcher, T. Alliston and V. M. Weaver, *Nat. Rev. Cancer*, 2009, **9**, 108–122; (*b*) S. Kumar and V. M. Weaver, *Cancer Metastasis Rev.*, 2009, **28**, 113–127.
7 T. G. Kuznetsova, M. N. Starodubtseva, N. I. Yegorenkov, S. A. Chizhik and R. I. Zhdanov, *Micron*, 2007, **38**, 824–833.
8 N. Wang, J. P. Butler and D. E. Ingber, *Science*, 1993, **260**, 1124–1127.
9 (*a*) M. Sato, N. Ohshima and R. Nerem, *J. Biomech.*, 1996, **29**, 461–467; (*b*) E. Evans and A. Yeung, Apparent viscosity and cortical tension of blood granulocytes determined by micropipet aspiration, *Biophys. J.*, 1989, **56**, 151–160.
10 (*a*) K. Svoboda, C. Schmidt, D. Branton and S. Block, *Biophys. J.*, 1992, **63**, 784–793; (*b*) S. Henon, G. Lenormand, A. Richert and F. Gallet, *Biophys. J.*, 1999, **76**, 1145–1151.
11 D. E. Discher, P. Janmey and Y.-L. Wang, *Science*, 2005, **310**, 1139–1143.
12 G. Popescu, K. Park, M. Mir and R. Bashir, *Lab Chip*, 2014, **14**, 646–652.
13 (*a*) K. Park, L. J. Millet, N. Kim, H. Li, X. Jin, G. Popescu, N. R. Aluru, K. J. Hsia and R. Bashir, *Proc. Natl. Acad. Sci. U. S. A.*, 2010, **107**, 20691–20696; (*b*) E. A. Corbin, L. J. Millet, K. R. Keller, W. P. King and R. Bashir, *Anal. Chem.*, 2014, **86**, 4864–4872; (*c*) M. Godin, F. F. Delgado, S. M. Son, W. H. Grover, A. K. Bryan, A. Tzur, P. Jorgensen, K. Payer, A. D. Grossman, M. W. Kirschner and S. R. Manalis, *Nat. Methods*, 2010, **7**, 387–390; (*d*) S. Son, A. Tzur, Y. Weng,

P. Jorgensen, J. Kim, M. W. Kirschner and S. R. Manalis, *Nat. Methods*, 2012, **9**, 910–912.

14 E. A. Corbin, L. J. Millet, J. H. Pikul, C. L. Johnson, J. G. Georgiadis, W. P. King and R. Bashir, *Biomed. Microdevices*, 2013, **15**, 311–319.

15 (*a*) R. Chotard-Ghodsnia and C. Verdier, in *Modeling of Biological Materials*, Springer, 2007, pp. 1–31; (*b*) A. N. Ketene, E. M. Schmelz, P. C. Roberts and M. Agah, *J. Nanomed. Nanotechnol.*, 2012, **8**, 93–102; (*c*) V. Vadillo-Rodriguez, S. R. Schooling and J. R. Dutcher, *J. Bacteriol.*, 2009, **191**, 5518–5525; (*d*) K. E. Bremmell, A. Evans and C. A. Prestidge, *Colloids Surf., B*, 2006, **50**, 43–48.

16 K. Park and R. Bashir, *Transducers*, Denver, CO, 2009.

17 (*a*) J. Hutter, J. Chen, W. Wan, S. Uniyal and M. Leabu, *Biol. Cell*, 2005, **219**, 61–68; (*b*) F. Braet, C. Rotsch, E. Wisse and M. Radmacher, *Appl. Phys. A: Mater. Sci. Process.*, 1998, **66**, S575–S578.

18 D. B. Agus, J. F. Alexander, W. Arap, S. Ashili, J. E. Aslan, R. H. Austin, V. Backman, K. J. Bethel, R. Bonneau, W.-C. Chen, C. Chen-Tanyolac, N. C. Choi, S. A. Curley, M. Dallas, D. Damania, P. C. W. Davies, P. Decuzzi, L. Dickinson, L. Estevez-Salmeron, V. Estrella, M. Ferrari, C. Fischbach, J. Foo, S. I. Fraley, C. Frantz, A. Fuhrmann, P. Gascard, R. A. Gatenby, Y. Geng, S. Gerecht, R. J. Gillies, B. Godin, W. M. Grady, A. Greenfield, C. Hemphill, B. L. Hempstead, A. Hielscher, W. D. Hillis, E. C. Holland, A. Ibrahim-Hashim, T. Jacks, R. H. Johnson, A. Joo, J. E. Katz, L. Kelbauskas, C. Kesselman, M. R. King, K. Konstantopoulos, C. M. Kraning-Rush, P. Kuhn, K. Kung, B. Kwee, J. N. Lakins, G. Lambert, D. Liao, J. D. Licht, J. T. Liphardt, L. Liu, M. C. Lloyd, A. Lyubimova, P. Mallick, J. Marko, O. J. T. McCarty, D. R. Meldrum, F. Michor, S. M. Mumenthaler, V. Nandakumar, T. V. O'Halloran, S. Oh, R. Pasqualini, M. J. Paszek, K. G. Philips, C. S. Poultney, K. Rana, C. A. Reinhart-King, R. Ros, G. L. Semenza, P. Senechal, M. L. Shuler, S. Srinivasan, J. R. Staunton, Y. Stypula, H. Subramanian, T. D. Tlsty, G. W. Tormoen, Y. Tseng, A. van Oudenaarden, S. S. Verbridge, J. C. Wan, V. M. Weaver, J. Widom, C. Will, D. Wirtz, J. Wojtkowiak and P.-H. Wu, *Sci. Rep.*, 2013, 3.

19 J. Rother, H. Nöding, I. Mey and A. Janshoff, *Open Biol.*, 2014, **4**, 140046.

20 T. Watanabe, H. Kuramochi, A. Takahashi, K. Imai, N. Katsuta, T. Nakayama, H. Fujiki and M. Suganuma, *J. Cancer Res. Clin. Oncol.*, 2012, **138**, 859–866.

21 I. J. Fidler, Biological behavior of malignant melanoma cells correlated to their survival in vivo, *Cancer Res.*, 1975, **35**, 218–224.

22 V. Palmieri, D. Lucchetti, A. Maiorana, M. Papi, G. Maulucci, G. Ciasca, M. Svelto, M. De Spirito and A. Sgambato, *Appl. Phys. Lett.*, 2014, **105**, 123701.

23 E. A. Corbin, B. R. Dorvel, L. J. Millet, W. P. King and R. Bashir, *Lab Chip*, 2014, **14**, 1401–1404.

24 M. Balland, N. Desprat, D. Icard, S. Féréol, A. Asnacios, J. Browaeys, S. Hénon and F. Gallet, *Phys. Rev. E: Stat., Nonlinear, Soft Matter Phys.*, 2006, **74**, 021911.